Molecular Dynamics Simulations of the Rotary Motor F_0 under External Electric Fields across the Membrane

Yang-Shan Lin,[†] Jung-Hsin Lin,[‡§¶*] and Chien-Cheng Chang[†¶]

[†]Institute of Applied Mechanics and [‡]School of Pharmacy, College of Medicine, National Taiwan University, Taipei, Taiwan; [§]Division of Mechanics, Research Center for Applied Science, Academia Sinica, Taipei, Taiwan; and [¶]Institute of Biomedical Sciences, Academia Sinica, Taipei, Taiwan

ABSTRACT The membrane-bound component F_0, which is a major component of the F_0F_1-ATP synthase, works as a rotary motor and plays a central role in driving the F_1 component to transform chemiosmotic energy into ATP synthesis. We conducted molecular dynamics simulations of b_2-free F_0 in a 1-palmitoyl-2-oleoyl-phosphatidylcholine lipid bilayer for tens of nanoseconds with two different protonation states of the *c*Asp-61 residue at the interface of the *a*-*c* complex in the absence of electric fields and under electric fields of ± 0.03 V/nm across the membrane. To our surprise, we observed that the upper half of the N-terminal helix of the c_1 subunit rotated about its axis clockwise by 30°. An energetic analysis revealed that the electrostatic repulsion between this N-terminal helix and subunit c_{12} was a major contributor to the observed rotation. A correlation map analysis indicated that the correlated motions of residues in the interface of the *a*-*c* complex were significantly reduced by external electric fields. The deuterium order parameter (S_{CD}) profile calculated by averaging all the lipids in the F_0-bound bilayer was not very different from that of the pure bilayer system, in agreement with recent ^{2}H solid-state NMR experiments. However, by delineating the lipid properties according to their vicinity to F_0, we found that the S_{CD} profiles of different lipid shells were prominently different. Lipids close to F_0 formed a more ordered structure. Similarly, the lateral diffusion of lipids on the membrane surface also followed a shell-dependent behavior. The lipids in the proximity of F_0 exhibited very significantly reduced diffusional motion. The numerical value of S_{CD} was anticorrelated with that of the diffusion coefficient, i.e., the more ordered lipid structures led to slower lipid diffusion. Our findings will help elucidate the dynamics of F_0 depending on the protonation state and electric field, and may also shed some light on the interactions between the motor F_0 and its surrounding lipids under physiological conditions, which could help to rationalize its extraordinary energy conversion efficiency.

INTRODUCTION

The H^+-ATP synthase is one of the molecular motors that have received a great deal of attention for a long time. This enzyme catalyzes the oxidative phosphorylation reaction for ATP synthesis. By hydrolyzing ATP, this enzyme can also function as a proton pump across the membrane. The H^+-ATP synthase can be divided into the membrane-bound component F_0 and the solvent-exposed component F_1. Some experiments have provided direct visualizations of the rotational motions of F_1 (1) and F_0 (2–4).

In electron spectroscopic images, the F_0 sector from *Escherichia coli* shows a deltoid-like structure (5). The F_0 complex $a_1b_2c_n$ can be reconstituted into phospholipid vesicles with proper proton translocation and F_1 binding properties (6). The symmetric mismatch between F_1 ($\alpha_3\beta_3$) and F_0 (c_{10-15}) seems to be melded by soft elastic power transmission (7–9) mediated by the stalk subunits γ and b_2 (10), and possibly contributions from other subunits. Reviews on the structure and function of F_0 have been published (11,12). It is recognized that the transmembrane voltage acting on the F_0 sector plays crucial roles in the function of ATP synthase (13). The transmembrane potential acts on the *c* ring, causing the rotational motion with respect to subunit *a*. It was recently verified that $\Delta\psi$ and ΔpH are equivalent driving forces for translocation of the proton across the biomembrane (14). Three types of F_0 subunits are required for proton conduction (6,15); however, the *b* subunits are believed to specifically contribute to energy storage, in the form of elastic energy. In *E. coli*, the two *b* subunits are identical and form a parallel α-helical coiled coil (16). The results of electron microscopic, cross-linking, and fluorescence resonance energy transfer experiments suggested that the b_2 subunits do not have direct contact with the *a*-*c* interface (17–19). More recent experiments showed that subunits *a* and *b* alone can form stable ab_2 complexes (20), which indirectly supports the notion that the b_2 subunits do not need to bind to the *c* ring. In addition, it was found that the transmembrane part of subunit *b* is sufficient for proton translocation activity, provided that the *a*-*c* complex has been preformed (21).

Despite the outstanding role played by this enzyme, investigations into the interactions of the F_0 component with the membrane lipid bilayer have been rather limited (22). In particular, there has been no simulation of the dynamics of F_0 with varying membrane potentials across the membrane. Previous steered molecular dynamics (MD) simulations of isolated F_1 (23) and isolated F_0 component (24) applied the torques along the molecular symmetric axis to accelerate the conformational changes and relative motions of the residues of proteins. As mentioned above, the pH gradient and the voltage difference across the inner membrane together

Submitted April 15, 2009, and accepted for publication November 13, 2009.

*Correspondence: jhlin@gate.sinica.edu.tw or jlin@ntu.edu.tw

Editor: Mark Girvin.

0006-3495/10/03/1009/9 $2.00

doi: 10.1016/j.bpj.2009.11.025

constitute the electrochemical potential, and therefore it remains of major interest to see the ''unsteered'' or ''natural'' behavior of F_0 in the presence of external electric fields.

At present, no x-ray crystallographic structure is available for the complete F_0 complex of the ATP synthase. The x-ray structures of the *c* ring of the F-type Na^+-ATPase from *Ilyobacter tartaricus* (25) and the *c* ring of H^+-ATP synthase from *Spirulina platensis* (26) are available, but the functional mechanism cannot be elucidated without the presence of the *a* subunit (27). To date, the model of the *a*-*c* complex constructed by Rastogi and Girvin (28) is the only structure of the membrane-bound F_0 section that contains these two essential elements for proton translocation. The protonation states of some important residues are crucial for the function of the F_0 sector. One essential amino acid residue is Asp-61 on the *c* subunit in all 12 copies (29,30). Deletion of this residue will abolish the enzyme activity (29). Another essential amino acid residue is Arg-210 of the *a* subunit. The Rastogi-Girvin model represents the *a*-*c* complex at pH 8, and Asp-61 of the *c* subunit nearest to the *a* subunit is not protonated.

In this study, we conducted MD simulations of this *a*-*c* complex model with an explicit lipid bilayer to refine the original model, and to investigate the behavior of water molecules in subunit *a* that were missing in the original protein-only model. We were particularly interested in observing the onset of helical motion in the *c* ring upon the change of the protonation state of Asp-61 of the c_1 subunit, which is the essential element of the Boyer's binding-change mechanism. To investigate the influence of transmembrane potential and pH gradient on the structure and dynamics of the *a*-*c* complex, we applied different electric fields along the membrane normal. A principal component analysis (PCA) and correlation map analysis were performed to extract important dynamical information about the system. To unravel the protein-lipid interactions in this system, we calculated the deuterium order parameter and later diffusion coefficients according to the lipid shells surrounding F_0.

MATERIALS AND METHODS

System setup of membrane-bound b_2-free F_0 systems

We adopted the model constructed based on NMR and chemical cross-linking data for F_0 (Protein Data Bank code: 1c17) published by Rastogi and Girvin (28), which encompasses both the *a* and *c* subunits. The entire b_2 subunit and the first 102 amino acids of the *a* subunit were not included in the Rastogi-Girvin model. However, this model included all the essential components for proton translocation. As noted above, experimental evidence indicates that the b_2 subunits may not have direct contact with the *a*-*c* interface. The missing N-terminal segment of the *a* subunit is also far from the *a*-*c* interface. This model represents a structure of b_2-free F_0 at a pH of 8, where the Asp-61 of the *c* subunit nearest to the *a* subunit is deprotonated. The F_0 component in this *c*Asp-61 protonation configuration is described as being in the ''locked'' state. In contrast, if all *c*Asp-61 residues are protonated, it is in the ''unlocked'' state.

In a previous study, the inner lumen of the *c* ring was found to be filled with phospholipids (31). However, the exact number of phospholipids within the *c* ring is not certain, and it may be dependent on the stoichiometry of the *c* subunits. We therefore tried to insert various numbers of lipid molecules, ranging from three to 10 lipids per monolayer, into the central cavity of the *c* ring. We found that, with seven lipid molecules for each monolayer in the inner lumen, the root mean-square deviation (RMSD) of the *c* ring from the original NMR structure after the 2-ns simulation was minimal. In all of these simulations, energy minimization was first carried out for 600 steps with the steepest-descent method. Then a 2-ns simulation at 315 K was performed with restraints on all of the protein atoms except hydrogen atoms, and finally another 2-ns simulation was carried out without restraints. Fig. 1 shows the equilibrated system with the *c* ring structure closest to the original Rastogi-Girvin model.

As depicted in Fig. 2, the cavity of the *c* subunit is well packed with lipids. It is worthwhile to mention that the *c* ring in the Rastogi-Girvin model is not perfectly circular, in contrast to the x-ray structure, which may reveal the structural influence of the *a* subunit on the *c* ring. Chlorine ions were added to neutralize the system. The final energy-minimized system was 147 × 129 × 85 $Å^3$ in size and included the ac_{12} complex, 451 1-palmitoyl-2-oleoyl-phosphatidylcholine (POPC) lipids, 25,247 water molecules, and 16 chlorine ions, yielding a total system of 109,378 atoms. The hydration level was ~56 water molecules per lipid. The protein/lipid molar ratio in our system is ~1:3, which is a very high protein concentration.

MD simulation protocols

After an 8-ns MD simulation without restraints, we applied an electric field in the *z* ($+E_z$) and negative *z* ($-E_z$) direction, respectively, to observe the effects of electric fields in different directions. The *z* axis is defined as the direction from the cytoplasmic side to the periplasmic side. The top side of the *c* ring, i.e., the binding site of F_1, is also pointing toward the *z* direction. The strength of electric field applied on to the membrane is 0.03 (V/nm), which is within the range of the physiological values (32,33). Three MD cases—one with no electric field (designated zero field), one with electric field $E_z = 0.03$ V/nm (designated E_z), and one other electric field $E_z = -0.03$ V/nm (designated $-E_z$)—were conducted for 12 ns for both proton configurations of *c*Asp-61 at the *a*-*c* interface. The total simulation time for the zero-field case was 20 ns. The dimensions of the three cases were 138.3 × 121.3 × 87.3 $Å^3$, 137.6 × 120.7 × 88.7 $Å^3$, and

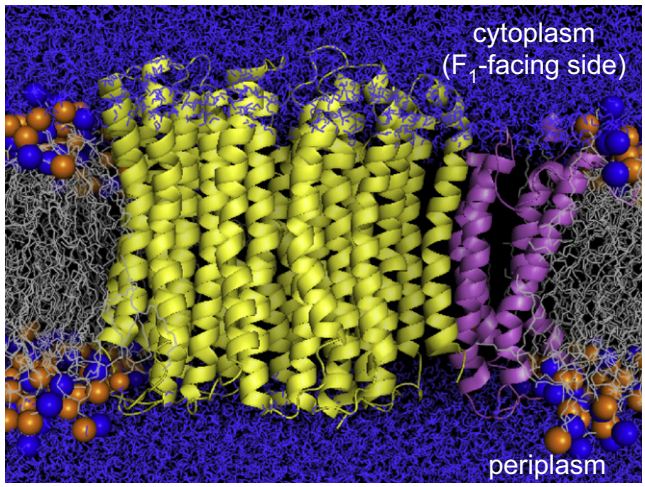

FIGURE 1 Molecular graphics of the simulation system of the rotary motor F_0 embedded in a POPC phospholipid bilayer in the explicit water environment. Yellow helices: *c* subunits; purple helices: *a* subunit; orange spheres: phosphate atom on the lipid headgroup; blue spheres: nitrogen atoms on the lipid headgroup; blue licorices: water molecules. The *z* direction is from the cytoplasmic side to the periplasmic side.

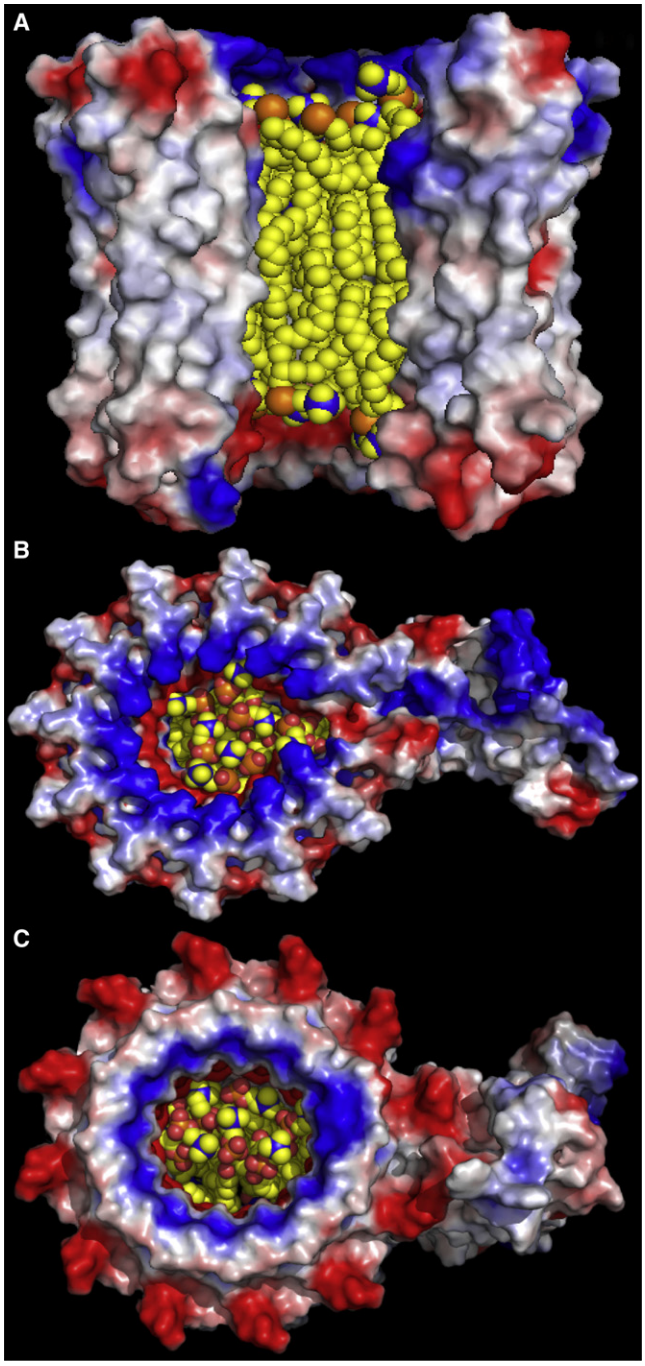

FIGURE 2 The *c* ring filled with lipids inside its central cavity. The *c* ring is represented by molecular surfaces colored by the electrostatic potential (*red* indicates negative potential, *blue* indicates positive). (*A*) Side view. The *c* ring is oriented in the direction in which the F_1 will bind from the top. Two *c* subunits were removed for better visual clarity. (*B*) Top view. (*C*) Bottom view. The lipids inside the *c* ring are closely packed.

$137.7 \times 120.8 \times 88.4$ Å^3, respectively. Other details of the simulation protocols are provided in the Supporting Material.

Definitions of lipid shells

It is conceivable that the nearness of lipids with respect to the F_0 protein is crucial for their structural and dynamical properties. The lipid shells were defined according to the van der Waals contacts with the more inner component of the system: the lipids are defined as the first shell if they have direct van der Waals contacts with the F_0 protein, as the second shell if they have direct van der Waals contact with the first shell lipids, and so on, which is similar to the hydration shells defined on the membrane surface (34). To avoid the boundary effect, lipids close to the simulation box boundaries were not selected. A total of five lipid shells were analyzed in this study.

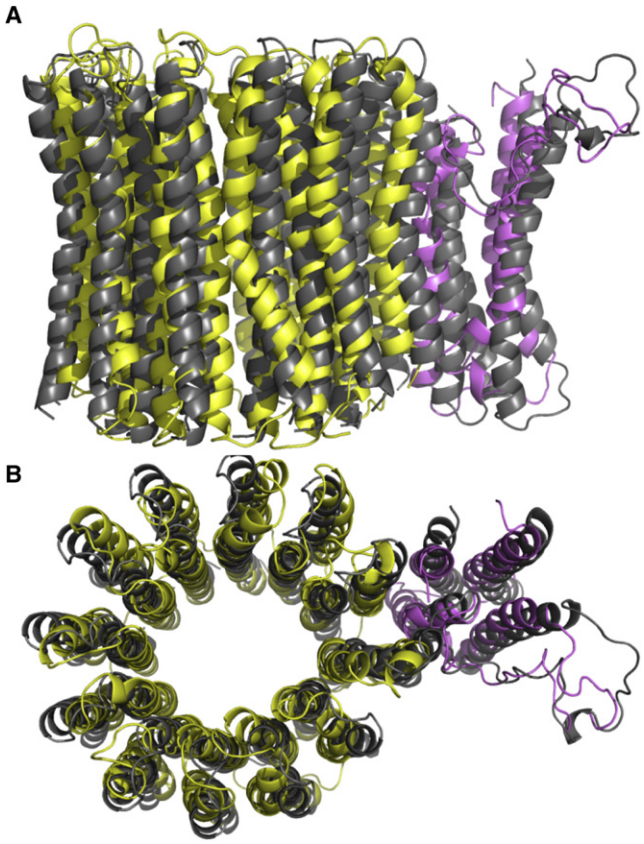

FIGURE 3 Structure alignment of F_0 in the locked state at the 8th-ns snapshot (*yellow* and *purple*) with the initial structure (the Rastogi-Girvin model). The RMSD is 3.208 Å. (*A*) Side view. (*B*) Top view.

RESULTS AND DISCUSSION

Stability and refinement of the Rastogi-Girvin model in the lipid bilayer

First, we investigated the locked-state F_0 system. In our simulations, the lipid bilayer structure remained intact and no water molecules permeated through the central region of the *c* ring, indicating close packing of the lipids within the inner lumen. Fig. 3 shows the structure alignment of the F_0 protein structure of the 8th-ns snapshot with the initial Rastogi-Girvin model.

The overall architectures of F_0 in different protonation states and under the electric fields in this study are remarkably stable. The RMSD of the α-carbon atoms of the F_0 protein and the *a* subunit only, and the radius of gyration of the *c* ring for the locked and unlocked cases can be found in Fig. S1 and Fig. S3.

TABLE 1 Average tilt angle (in degrees) of each *c* subunit in the locked state

Subunit	Initial structure	$E_z = 0$ V/nm	$E_z = 0.03$ V/nm	$E_z = -0.03$ V/nm
c_1	5.990	9.610	9.868	9.887
c_2	1.070	3.518	3.472	3.663
c_3	2.999	3.428	2.400	2.521
c_4	4.854	4.963	4.643	4.791
c_5	6.318	2.860	2.276	3.192
c_6	7.640	3.662	4.697	6.266
c_7	8.132	5.220	6.779	8.702
c_8	7.678	5.687	6.375	7.111
c_9	6.841	4.577	4.737	6.322
c_{10}	5.399	6.574	7.309	8.571
c_{11}	4.757	5.935	6.461	7.428
c_{12}	3.955	6.034	5.314	6.101

Trajectories from the 8th to the 20th ns were taken to average the tilt angles.

The tilt angles (defined as the helical axis of each subunit c_n with respect to the membrane normal) are listed in Table 1. The helical axis can be determined by calculating the longest eigenvector of the moment of inertia tensor. After the MD simulation, the tilt angles of seven units (c_1–c_4 and c_{10}–c_{12}) become slightly larger than those of the original structure. These subunits are closer to the *a* subunit than the other five subunits (c_5–c_9) with decreased tilt angles, reflecting the influence of asymmetry due to the presence of the *a* subunit. The effect of external electric fields is only modest.

In each *c* subunit, both the N- and C-terminal helices are bent due to the presence of Gly-23 and Pro-64, respectively. The kink angles for each *c* subunit are shown in Table 2. After the MD simulation, the kink angles of each C-terminal helix of the *c* subunits, except for the c_1 and c_2 subunits, became larger. On the other hand, the kink angle of the N-terminal helix of each *c* subunit did not change significantly after the simulation.

Four histograms of the distance between the atom pairs of the residues that may lie on the possible proton translocation pathways within the *a* subunit (35,36) are provided in Fig. S10 and Fig. S11. The hydrogen bond between Asp-61 and Arg-210 is more stable when F_0 is in the locked state. Histogram analyses of the pair distance between residues that lie on the proton translocation pathways can also be obtained from Fig. S13.

Rotation of the N-terminal helix of the c_1 subunit

Fig. 4 illustrates the locations of Ala-24, Ile-28, and Asp-61 in subunits c_1 and c_{12} of the original Rastogi-Girvin model, in the final snapshot of the locked state without electric field, the final snapshot of the unlocked state without electric field, and the final snapshot of the unlocked state in the presence of electric field $+E_z$, respectively. It reveals that the conformation transition of the N-terminal (or TM1) helix of the c_1 subunit occurred after Asp-61 was protonated. Fig. S18 depicts the time course of the angle between the two normal vectors of the planes, defined by the α-carbon atoms of the three residues (Ala-24, Ile-28, and Asp-61), in the initial Rastogi-Girvin model and the MD snapshot. To confirm that this conformational transition of the N-terminal helix of the c_1 subunit was reproducible, two more simulations with different initial velocities on each atom were conducted. Both additional simulations confirmed the rotation of the upper part of the N-terminal helix. On the contrary, however, the C-terminal helix of the c_1 subunit did not appear to undergo significant conformational changes in these simulations. If the rotation of the C-terminal helix is required for the function of F_0, as proposed by Rastogi and Girvin (28), the rotation of the N-terminal helix observed in the simulation may reflect the existence of an intermediate state. In contrast, when the F_0 is in the locked state, the relative locations of Ala-24, Ile-28, and Asp-61 remain intact and do not depend on the applied electric fields.

To further determine whether the N-terminal helix was rotated altogether or twisted at the hinge residue Gly-23, we performed a PCA. Because the conformational transition described in Fig. S18 reached its final state in ~2 ns, only this period of simulations was analyzed by PCA, and the

TABLE 2 Average kink angles between the two bent segments of the N- or C-terminal helices

Subunit	Initial N	Structure C	$E_z = 0$ N	V/nm C	$E_z = 0.03$ N	V/nm C	$E_z = -0.03$ N	V/nm C
c_1	9.692	29.288	17.605	24.445	15.524	21.412	14.374	21.374
c_2	8.814	19.962	17.573	9.887	17.770	8.282	15.794	9.490
c_3	8.779	20.028	16.913	35.332	18.945	32.165	20.036	35.313
c_4	8.818	20.021	16.237	31.389	16.938	32.749	16.020	32.588
c_5	8.663	19.916	16.374	33.750	19.842	33.881	19.633	36.767
c_6	8.769	19.934	11.225	25.610	9.833	22.394	10.770	28.376
c_7	8.518	20.017	6.362	37.131	6.385	33.860	6.920	32.132
c_8	8.605	20.052	7.518	35.487	11.328	37.731	7.390	32.173
c_9	8.812	19.848	9.610	30.132	10.468	29.588	9.678	32.719
c_{10}	8.607	19.923	13.641	22.707	14.964	24.741	15.117	17.609
c_{11}	8.763	19.989	13.825	30.528	14.960	29.489	14.145	28.869
c_{12}	8.899	19.907	7.387	29.231	5.728	34.164	7.538	37.824

The two segments of the N-terminal helices are from Asn-3 to Gly-23 and from Gly-23 to Gly-38, and the two segments of the C-terminal helices are from Ile-46 to Pro-64 and from Pro-64 to Val-74.

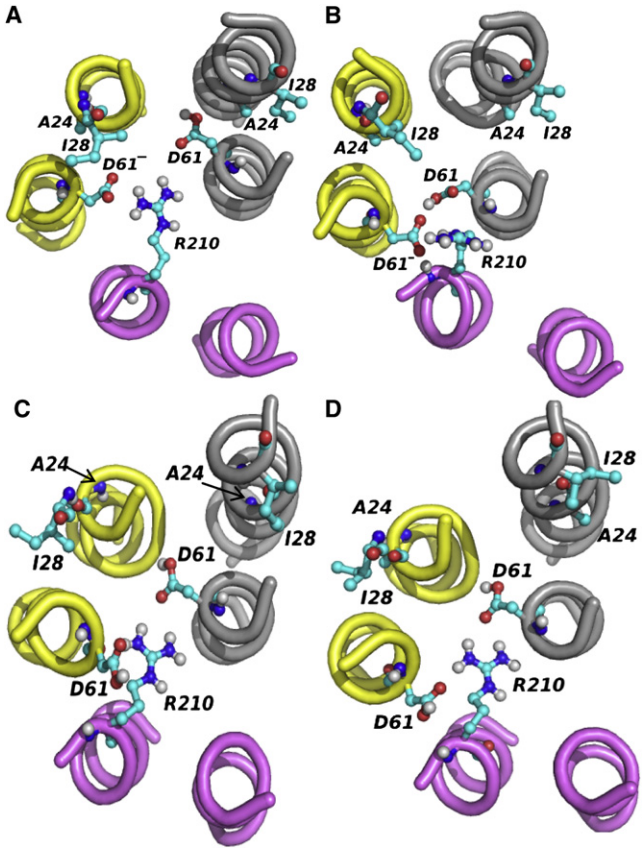

FIGURE 4 Locations of c_1 (*yellow*), c_{12} (*gray*), and a_4 and a_5 subunits of the *a-c* complex of the initial structure and final structures of the MD simulations. (*A*) Initial structure. (*B*) $E_z = 0$ V/nm, locked state. (*C*) $E_z = 0$ V/nm, unlocked state. (*D*) $E_z = 0.03$ V/nm, unlocked state. Asp-61, Ala-24, Ile-28, and Arg-210 are shown in sticks and balls.

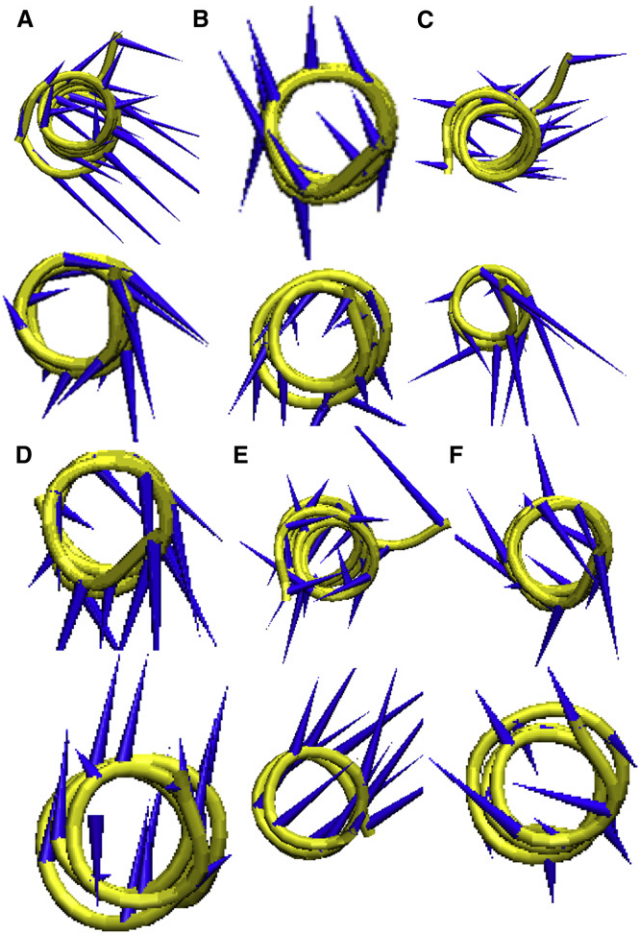

FIGURE 5 Porcupine plots of three MD simulations in the unlocked state based on the PCA-1 eigenvector projected on the membrane plane for the two segments of the N-terminal (*A*, *C*, and *E*) and C-terminal (*B*, *D*, and *F*) helices of c_1, viewed from the top. (*A* and *B*) $E_z = 0$ V/nm. (*C* and *D*) $E_z = 0.03$ V/nm. (*E* and *F*) $E_z = -0.03$ V/nm. Residue number of the two segments of the N-terminal helix: 1–23 (up) and 24–36 (down). Residue number of the two segments of the C-terminal helix: 51–64 (up) and 65–79 (down).

corresponding porcupine plots were made. The porcupine plots illustrate the direction and magnitude of the covariance vectors on the α-carbon atom of each residue (37,38). Fig. 5 shows the top views of porcupine plots of two segments of the c_1 subunit based on the PCA-1 eigenvector projected on the membrane plane. The porcupine plots illustrate that the N-terminal helix of c_1 subunit has undergone a twisting motion.

It is important to delineate which factors caused Ala-24 and Ile-28 to move away from Asp-61. We therefore calculated the Coulomb and van der Waals energies between the TM1 of the c_1 subunit and the surrounding helices (shown in Fig. S15, Fig. S16, and Fig. S17), including the c_{12} and c_2 subunits, as well as the a_4 and a_5 helices. We found that the Coulomb interaction between the c_1 TM1 and the c_{12} subunit provides the major repulsive force for the TM1 of the c_1 subunit to become twisted. To identify which residues of the c_{12} subunit contribute to the repulsion, we calculated the energies between the TM1 of the c_1 subunit and each residue of c_{12} subunit, as shown in Fig. S17, and found that Asp-61 and Lys-34 of the c_{12} subunit are the two essential residues that induced the twisting motion of the N-terminal helix of the c_1 subunit.

Correlation map analysis of residue pairs in the interface of the *a-c* complex

The correlation maps for the relative motions between the residue pairs of the c_1, c_{12} subunits and TM4, TM5 of subunit *a* (*a*TM4 and *a*TM5) for the unlocked case were calculated to further analyze the effects caused by electric fields. The correlation coefficients of these interfacial residues are shown in Fig. 6, *A–C*. It can be observed very clearly that external electric fields reduce the residue-residue correlations significantly. This observation is further supported in a more quantitative manner by the histogram analysis of correlation coefficients, shown in Fig. 6 *E*. The loss of correlated motions in the presence of electric fields may

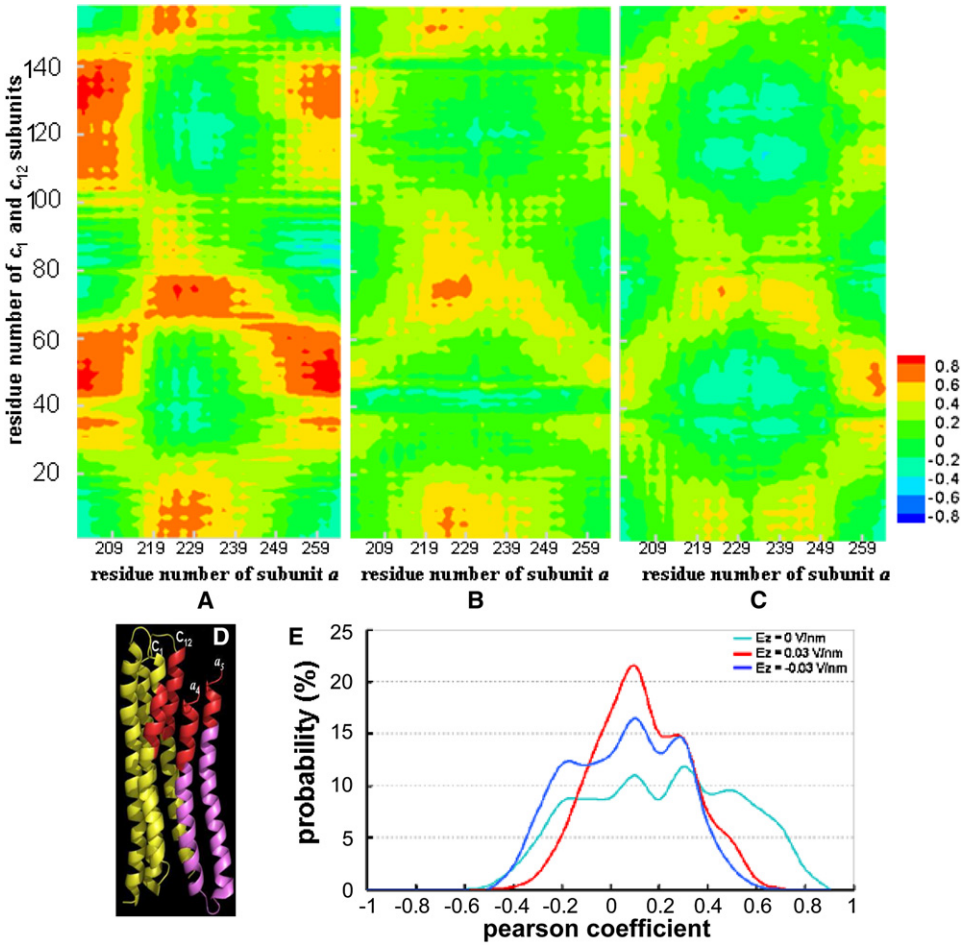

FIGURE 6 Residue-residue correlation maps for the unlocked cases. (*A*) $E_z = 0$ V/nm. (*B*) $E_z = 0.03$ V/nm. (*C*) $E_z = -0.03$ V/nm. The residue numbers of the c_1 and c_2 subunits are 1–79 and 80–158, respectively. High correlation is indicated by coefficients approaching +1, anticorrelation is indicated by coefficients approaching −1. (*D*) Locations of highly correlated residues (residue number of c_1: 44–56; c_{12}: 128–136; a_4: 199–209; a_5: 258–265), which are in red. (*E*) Histogram of correlation maps.

imply that F_0 is less stable or more mobile under such conditions. The case of $E_z = -0.03$ V/nm exhibited the largest reduction for the correlated motion. Of interest, this case actually corresponds to the functioning state, in view of the transmembrane potential, of this motor for ATP synthesis. Fig. 6 *D* shows that the highly correlated residues are near the cytoplasm side. As shown in Fig. 2, *B* and *C*, the surface electrostatic potential of the c_1 and c_{12} subunits is opposite to the surface potential of *a*TM4 and *a*TM5 for the region near the cytoplasm. Thus, electrostatic attraction plays an important role in this highly correlated motion, which also explains why external electric fields can regulate such correlated motions.

In the locked state, the magnitudes of the residue-residue correlated motions were higher than those of the unlocked state, and the reduction of correlated motions due to electric fields was less, as can be seen in Fig. S7.

Deuterium order parameters S_{CD}

As a reference, we first calculated the S_{CD} profile of the bilayer with 512 POPC lipids and the S_{CD} profile of all the lipids with F_0 embedded in the membrane. In Fig. 7 *A*, it can be seen that the two S_{CD} curves are quite similar (for simplicity, only the *sn*-1 chain is shown). It should be stressed that the effect of the F_0 protein is small even though the protein/lipid molar ratio is high, which is in good agreement with recent NMR experimental data (22). Fig. 7 *B* shows the S_{CD} profile of all the lipids in the presence of electric fields. Again, these two S_{CD} profiles of all the lipids are still not very different from the cases of zero fields. Therefore, the S_{CD} profile calculated by averaging over all the lipids does not resolve the differences among these systems.

To achieve a finer resolution for dissecting the interactions among lipids, F_0, and the influence of external electric fields, we then calculated the S_{CD} profiles for different shells of lipids. The S_{CD} profiles of lipids in different shells are shown in Fig. 8. Lipids inside the *c*-subunit and the lipids belonging to the first shell are more ordered, which is even more prominent for the MD simulation with electric field from the cytoplasmic side to the periplasmic side, i.e., the case of Ez = +0.03 V/nm. Lipids outside the second shell have a shallower S_{CD} profile compared to the case of pure bilayer. Thus, our results indicate that the F_0 protein has the effect of increasing the deuterium order parameter of the lipids adjacent to it. Due to tight packing, lipids inside the *c*-subunit are the most ordered. The S_{CD} profile of lipids in the second shell is similar to that of lipids far away from F_0. It is

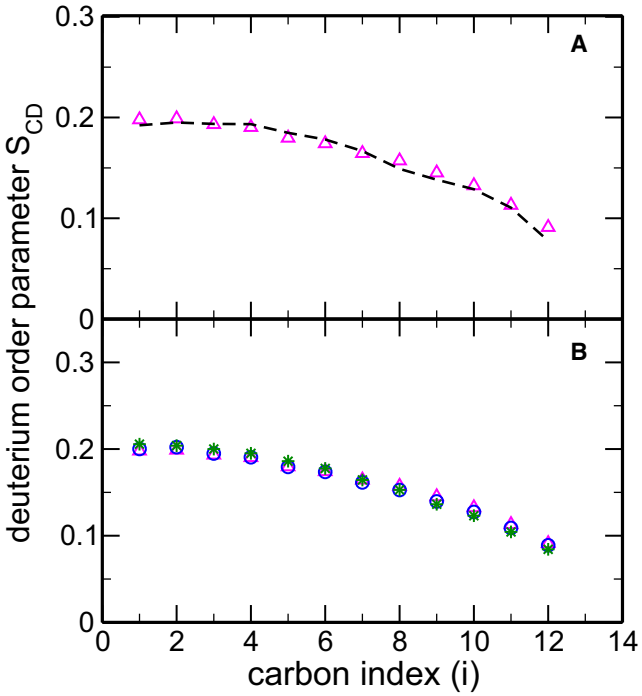

FIGURE 7 (*A*) Comparison of the deuterium order parameter profiles based on averaging all the lipids in the F_0-embedded membrane from the zero-field simulation (Δ) and pure bilayer simulation (*dashed curve*). (*B*) Comparison of the deuterium order parameter profiles based on averaging all the lipids in the F_0-embedded membrane for three MD simulations (zero field, Δ; $+E_z$, ○; $-E_z$, *).

anticipated that the S_{CD} profile of the third shell (or also the fourth shell) should reveal a less ordered lipid structure, because we previously showed that the S_{CD} profile of all the lipids is similar to that of the pure bilayer case, and therefore if the first shell lipids are more ordered, the lipids of some other shells should be more disordered so that the overall S_{CD} profile will be the same. These S_{CD} profiles indeed behaved as expected, as shown in Fig. 8, *C* and *D*.

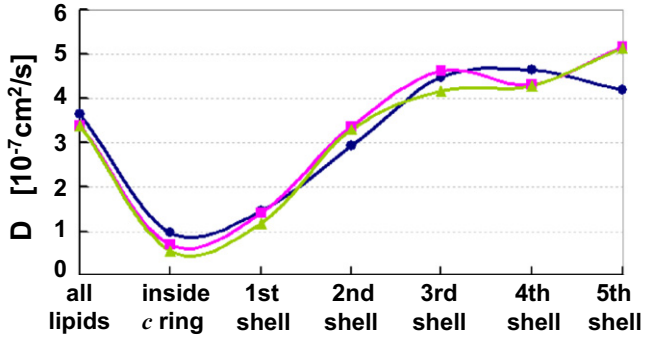

FIGURE 9 Lateral diffusion coefficient profiles of lipids in different shells surrounding the *c* ring or within the *c* ring. Blue curve: zero field; magenta curve: $+E_z$, green curve: $-E_z$.

Lateral diffusion of lipids

The lateral diffusion coefficients of different shell lipids for three MD cases are shown in Fig. 9.

In comparison to the reference value, the presence of the F_0 sector in the membrane reduced the diffusion motion of lipids. The diffusion coefficient of lipids inside the *c* ring was smallest because of the compactness of this space. The diffusion coefficients increased when the distance between the lipids and F_0 increased. The diffusion coefficients of lipids far away from F_0 for MD cases with electric fields were similar to the value of the pure bilayer. This means that the finite size effect is negligible. The profiles also reveal that the diffusion coefficients of lipids in the second shell were similar to the averaged value of all lipids in the

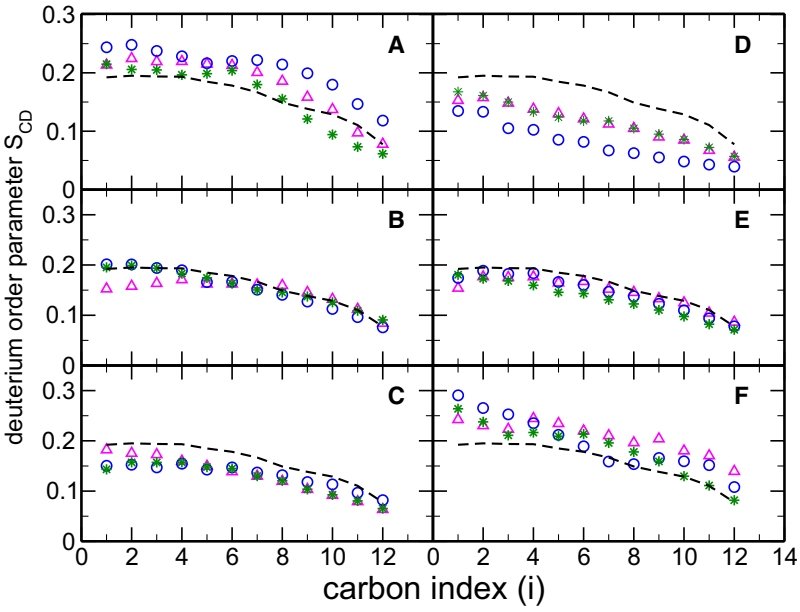

FIGURE 8 Deuterium order parameter profile of the lipids in different shells surrounding the *c* ring. (*A*) First shell. (*B*) Second shell. (*C*) Third shell. (*D*) Fourth shell. (*E*) Fifth shell. (*F*) Lipids inside the *c* ring. The symbols are as described in Fig. 7.

F_0-bound membrane system. The lipids in the third and fourth shells also exhibited enhanced diffusional motion. The numerical value of S_{CD} appears to be anticorrelated with that of the diffusion coefficient, and we obtained a consistent physical picture: if the lipids form a more ordered structure, they will exhibit reduced diffusional motion. Furthermore, the existence of the ordered, less-diffusive, lipid-shell structures may help to lubricate the rotational motion of the *c* ring.

CONCLUSIONS

In this work, we conducted MD simulations to examine the stability of the Rastogi-Girvin model of the *a*-*c* complex of the F_0 section of the motor. We found that the overall architecture of the Rastogi-Girvin model was maintained, whereas a twisting motion of the N-terminal helix of the c_1 subunit was observed by means of PCA and porcupine plots. A correlation map analysis revealed that external electric fields reduced the residue-reside correlations. We hypothesize that the twist of the N-terminal helix of the c_1 subunit in the protonated form may be a necessary intermediate state in progressing toward the larger conformational transitions.

The NMR deuterium order parameter profile calculated from all the lipids in the F_0-bound membrane of our simulations agrees with recent experimental results (22). Further analyses of the order parameter profiles, height profiles, and lateral diffusion revealed very interesting shell structures of lipids. Such shell structures of lipids remain in the presence of electric fields, irrespective of their directions. We believe that the lipid shell structure surrounding the *c* ring, along with its structural and dynamical properties, can provide new insights into the remarkable efficiency of the rotational catalysis of ATP synthase.

SUPPORTING MATERIAL

Details of the simulation protocols, 18 figures, and more references are available at http://www.biophysj.org/biophysj/supplemental/S0006-3495(09)01754-8.

We thank Prof. Tian-Yow Tsong of the University of Minnesota for many inspiring discussions, and the National Center for High Performance Computing of Taiwan for its generous support of this study. J.H.L. thanks Dr. Thomas Meier of the Max Planck Institute for Biophysics (Frankfurt, Germany) for many fruitful discussions.

This study was supported by the Research Center for Applied Science, Academia Sinica. J.H.L. was funded by the National Science Council of Taiwan under contracts NSC 97-2923-M-001-001-MY3, 96-2627-B-002-004, and 95-2112-M-002 -007.

REFERENCES

1. Noji, H., R. Yasuda, …, K. Kinosita, Jr. 1997. Direct observation of the rotation of F1-ATPase. *Nature*. 386:299–302.
2. Sambongi, Y., Y. Iko, …, M. Futai. 1999. Mechanical rotation of the *c* subunit oligomer in ATP synthase (F0F1): direct observation. *Science*. 286:1722–1724.
3. Tanabe, M., K. Nishio, …, M. Futai. 2001. Rotation of a complex of the γ subunit and *c* ring of *Escherichia coli* ATP synthase. The rotor and stator are interchangeable. *J. Biol. Chem.* 276:15269–15274.
4. Ueno, H., T. Suzuki, …, M. Yoshida. 2005. ATP-driven stepwise rotation of FoF1-ATP synthase. *Proc. Natl. Acad. Sci. USA*. 102:1333–1338.
5. Birkenhäger, R., M. Hoppert, …, K. Altendorf. 1995. The F_0 complex of the *Escherichia coli* ATP synthase. Investigation by electron spectroscopic imaging and immunoelectron microscopy. *Eur. J. Biochem.* 230:58–67.
6. Altendorf, K., W. D. Stalz, …, G. Deckers-Hebestreit. 2000. Structure and function of the F_0 complex of the ATP synthase from *Escherichia coli*. *J. Exp. Biol.* 203:19–28.
7. Junge, W., O. Pänke, …, S. Engelbrecht. 2001. Inter-subunit rotation and elastic power transmission in F_0F_1-ATPase. *FEBS Lett.* 504: 152–160.
8. Sielaff, H., H. Rennekamp, …, W. Junge. 2008. Domain compliance and elastic power transmission in rotary F_0F_1-ATPase. *Proc. Natl. Acad. Sci. USA*. 105:17760–17765.
9. Pänke, O., D. A. Cherepanov, …, W. Junge. 2001. Viscoelastic dynamics of actin filaments coupled to rotary F-ATPase: angular torque profile of the enzyme. *Biophys. J.* 81:1220–1233.
10. Neukirch, S., A. Goriely, and A. C. Hausrath. 2008. Elastic coiled-coils act as energy buffers in the ATP synthase. *Int. J. Non-linear Mech.* 43:1064–1073.
11. Deckers-Hebestreit, G., and K. Altendorf. 1996. The F_0F_1-type ATP synthases of bacteria: structure and function of the F_0 complex. *Annu. Rev. Microbiol.* 50:791–824.
12. Junge, W., H. Sielaff, and S. Engelbrecht. 2009. Torque generation and elastic power transmission in the rotary F_0F_1-ATPase. *Nature*. 459:364–370.
13. Kaim, G., and P. Dimroth. 1999. ATP synthesis by F-type ATP synthase is obligatorily dependent on the transmembrane voltage. *EMBO J.* 18:4118–4127.
14. Wiedenmann, A., P. Dimroth, and C. von Ballmoos. 2008. $\Delta\psi$ and ΔpH are equivalent driving forces for proton transport through isolated F0 complexes of ATP synthases. *Biochim. Biophys. Acta*. 1777:1301–1310.
15. Schneider, E., and K. Altendorf. 1985. All three subunits are required for the reconstitution of an active proton channel (F_0) of *Escherichia coli* ATP synthase (F_1F_0). *EMBO J.* 4:515–518.
16. Del Rizzo, P. A., Y. M. Bi, and S. D. Dunn. 2006. ATP synthase *b* subunit dimerization domain: a right-handed coiled coil with offset helices. *J. Mol. Biol.* 364:735–746.
17. Düser, M. G., Y. M. Bi, …, M. Börsch. 2008. The proton-translocating *a* subunit of F_0F_1-ATP synthase is allocated asymmetrically to the peripheral stalk. *J. Biol. Chem.* 283:33602–33610.
18. Wilkens, S., and R. A. Capaldi. 1998. ATP synthase's second stalk comes into focus. *Nature*. 393:29.
19. Fillingame, R. H., W. Jiang, and O. Y. Dmitriev. 2000. Coupling $H(^+)$ transport to rotary catalysis in F-type ATP synthases: structure and organization of the transmembrane rotary motor. *J. Exp. Biol.* 203:9–17.
20. Stalz, W. D., J. C. Greie, …, K. Altendorf. 2003. Direct interaction of subunits *a* and *b* of the F_0 complex of *Escherichia coli* ATP synthase by forming an ab_2 subcomplex. *J. Biol. Chem.* 278:27068–27071.
21. Greie, J. C., T. Heitkamp, and K. Altendorf. 2004. The transmembrane domain of subunit *b* of the *Escherichia coli* F_1F_0 ATP synthase is sufficient for H^+-translocating activity together with subunits *a* and *c*. *Eur. J. Biochem.* 271:3036–3042.
22. Kobayashi, M., A. V. Struts, …, H. Akutsu. 2008. Fluid mechanical matching of H^+-ATP synthase subunit *c*-ring with lipid membranes revealed by ^2H solid-state NMR. *Biophys. J.* 94:4339–4347.
23. Böckmann, R. A., and H. Grubmüller. 2002. Nanoseconds molecular dynamics simulation of primary mechanical energy transfer steps in F_1-ATP synthase. *Nat. Struct. Biol.* 9:198–202.

24. Aksimentiev, A., I. A. Balabin, …, K. Schulten. 2004. Insights into the molecular mechanism of rotation in the F_o sector of ATP synthase. *Biophys. J.* 86:1332–1344.

25. Meier, T., P. Polzer, …, P. Dimroth. 2005. Structure of the rotor ring of F-type Na^+-ATPase from *Ilyobacter tartaricus*. *Science*. 308:659–662.

26. Pogoryelov, D., O. Yildiz, …, T. Meier. 2009. High-resolution structure of the rotor ring of a proton-dependent ATP synthase. *Nat. Struct. Mol. Biol.* 16:1068–1073.

27. Valiyaveetil, F. I., and R. H. Fillingame. 1997. On the role of Arg-210 and Glu-219 of subunit *a* in proton translocation by the *Escherichia coli* F_0F_1-ATP synthase. *J. Biol. Chem.* 272:32635–32641.

28. Rastogi, V. K., and M. E. Girvin. 1999. Structural changes linked to proton translocation by subunit c of the ATP synthase. *Nature*. 402: 263–268.

29. Junge, W., H. Lill, and S. Engelbrecht. 1997. ATP synthase: an electrochemical transducer with rotatory mechanics. *Trends Biochem. Sci.* 22:420–423.

30. Elston, T., H. Y. Wang, and G. Oster. 1998. Energy transduction in ATP synthase. *Nature*. 391:510–513.

31. Oberfeld, B., J. Brunner, and P. Dimroth. 2006. Phospholipids occupy the internal lumen of the *c* ring of the ATP synthase of *Escherichia coli*. *Biochemistry*. 45:1841–1851.

32. Teissie, J., B. E. Knox, …, J. Wehrle. 1981. Synthesis of adenosine triphosphate in respiration-inhibited submitochondrial particles induced by microsecond electric pulses. *Proc. Natl. Acad. Sci. USA*. 78: 7473–7477.

33. Liu, D. S., R. D. Astumian, and T. Y. Tsong. 1990. Activation of Na^+ and K^+ pumping modes of (Na,K)-ATPase by an oscillating electric field. *J. Biol. Chem.* 265:7260–7267.

34. Lin, J. H., N. A. Baker, and J. A. McCammon. 2002. Bridging implicit and explicit solvent approaches for membrane electrostatics. *Biophys. J.* 83:1374–1379.

35. Angevine, C. M., and R. H. Fillingame. 2003. Aqueous access channels in subunit *a* of rotary ATP synthase. *J. Biol. Chem.* 278:6066–6074.

36. Angevine, C. M., K. A. G. Herold, and R. H. Fillingame. 2003. Aqueous access pathways in subunit *a* of rotary ATP synthase extend to both sides of the membrane. *Proc. Natl. Acad. Sci. USA*. 100: 13179–13183.

37. Tai, K., T. Y. Shen, …, J. A. McCammon. 2002. Mechanism of acetylcholinesterase inhibition by fasciculin: a 5-ns molecular dynamics simulation. *J. Am. Chem. Soc.* 124:6153–6161.

38. Tai, K., T. Y. Shen, …, J. A. McCammon. 2001. Analysis of a 10-ns molecular dynamics simulation of mouse acetylcholinesterase. *Biophys. J.* 81:715–724.